ISET Journal of Earthquake Technology, Paper No. 405, Vol. 37, No. 4, December 2000, pp. 119-142

SHAKING TABLE TESTING OF RC WALLS

R. Pinho

Department of Civil and Environmental Engineering
Imperial College, Imperial College Road, London SW7 2BU, UK

ABSTRACT

Several large-scale wall specimens were recently tested under dynamic conditions on the shaking-table at LNEC (Lisbon). The main objective of this experimental programme was to assess the effectiveness of selective intervention techniques for repair and strengthening of reinforced concrete walls. The models were tested up to collapse using both artificial and natural accelerograms. In this paper, a detailed description of the set-up of the experiments is presented. Different test-rig configurations are discussed, highlighting the advantages and drawbacks of each solution, and justifying the selection of the scheme adopted. Scaling issues are also analysed in detail and their implication on choice of materials, test set-up and choice of input motion is discussed. This is followed by a summary of the procedure employed in the design of the models together with an overview of the model construction process and test sequence.

KEYWORDS: Shaking-Table, Testing, RC Walls, Retrofitting

INTRODUCTION

Although, according to Aristizabal-Ochoa and Clark (1980), attempts at testing structures under earthquake loading have been recorded as early as at the turn of century (Rogers, 1908), it was not until the late 60's and early 70's that effective shaking-table testing of structural models started to be carried out. This came as a result of the advances in electro-hydraulic servo equipment, as well as improvements in computer hardware and instrumentation, for control and acquisition of data (Aristizabal-Ochoa and Clark, 1980).

Such work was mainly initiated in the US in the late 60's and early 70's, with the set-up of dynamic testing facilities at the University of Illinois Urbana (Sozen et al., 1969; Otani and Sozen, 1972) and University of California Berkeley in 1971 (Bouwkamp et al., 1971; Rea and Penzien, 1972). Since then, shaking table testing has been widely adopted in earthquake engineering research centres worldwide, reflecting the fact that such experimental method remains as the only tool capable of truly reproducing the dynamic effects that earthquakes impose on structures. In fact, notwithstanding the practicality and effectiveness of pseudo-dynamic testing, the important effects introduced by strain-rate in the structural response of structures continue to raise doubts regarding the suitability of static or quasi-static methods for studying the dynamic behaviour of structures under earthquake loading (Paulson and Abrams, 1990).

On the other hand, however, hydraulic power limitations in the vast majority of currently available shaking tables impose the requirement for the use of reduced scale specimens. This, in turn, introduces difficulties and uncertainty in the interpretation of experimental results, since it has yet to be established what is the minimum scale and minimum substructure portion of a building system that can be tested to reflect strength and deformation properties of actual buildings (Abrams, 1996).

Therefore, the need for building large and powerful dynamic facilities, capable of testing up to failure full-scale models, has become clear, and thus considerable effort and funding has been placed over the past 40 years in the construction of continuously larger and more powerful shaking table facilities around the world. As an example, the National Research Institute for Earth Science and Disaster Prevention in Tukuba (Japan) currently runs a 15×14.5 m^2 table with a maximum weight capacity of 500 tonnes, under which peak velocities and accelerations of 100 cm/s and 0.5 g, respectively, can be achieved (Yamada et al., 2000), together with a peak displacement of 22 cm. Such characteristics do represent a significant advance over those of the pioneering facilities at the University of Illinois Urbana: a 3.65×3.65 m^2 featuring a loading capacity of 4.5 tonnes (Sozen et al., 1969).

Despite such advances, testing of full-scale structures under dynamic loading, such as those reported by Minowa et al. (1995), is still far from being a common undertaking, mainly related due to the very high cost associated to such work. However, if applied to isolated structural members (or sub-assemblies), for which large-scale models can be more easily employed, such type of testing is, in principle, most suitable to accurately reproduce the seismic response of these elements. In the particular case of structural walls, shaking table testing has been relatively common over the past two decades, with both small- and large-scale models being tested under dynamic loading (e.g., Rothe and Kōnig, 1988; Farrar and Baker, 1993; Lu and Wu, 1996; Inoue et al., 1997).

In the present paper, the experimental work carried at the Centre for Earthquake Engineering Studies and Equipment at LNEC (Lisbon, Portugal), under the auspices of the ECOEST II (European Consortium of Earthquake Shaking Tables), is described. Eight large-scale wall models were tested up to collapse, using both artificial and natural accelerograms, to assess the effectiveness of the application of selective techniques (Elnashai, 1992) for repair and strengthening of RC walls under dynamic loading. The feasibility and efficiency of such retrofitting methods had already been experimentally assessed under static loading (Elnashai and Salama, 1992), and analytically verified through numerical studies (Elnashai and Pinho, 1998). However, uncertainties regarding their behaviour when subjected to dynamic strain rates called for further testing under dynamic loading conditions. Further, verification of previously derived design formulae needed also validation under such type of loading. Therefore, the present experimental programme was devised and carried out.

Hereafter, a detailed description of the set-up of the experiments is presented. Different test-rig configurations are discussed, highlighting the advantages and drawbacks of each solution, and justifying the selection of the scheme adopted. Scaling issues are also analysed in detail and their implication on choice of materials, test set-up and choice of input motion is discussed. This is followed by a summary of the procedure employed in the design of the models together with an overview of the model construction process and test sequence. A thorough and detailed account of the test results is beyond the scope of this paper, where focus is on the experimental method. Such comprehensive review of results can nevertheless be found elsewhere (Elnashai et al., 2000).

TEST SET-UP

1. Characteristics of the Shaking Table

The 3D shaking table at LNEC is capable of testing structures under three translational orthogonal degrees of freedom (i.e. two horizontals and one vertical). The three rotational degrees of freedom (i.e. roll, pitch and yaw) are constrained by torque tubes systems, one for each degree, as shown in Figure 1.

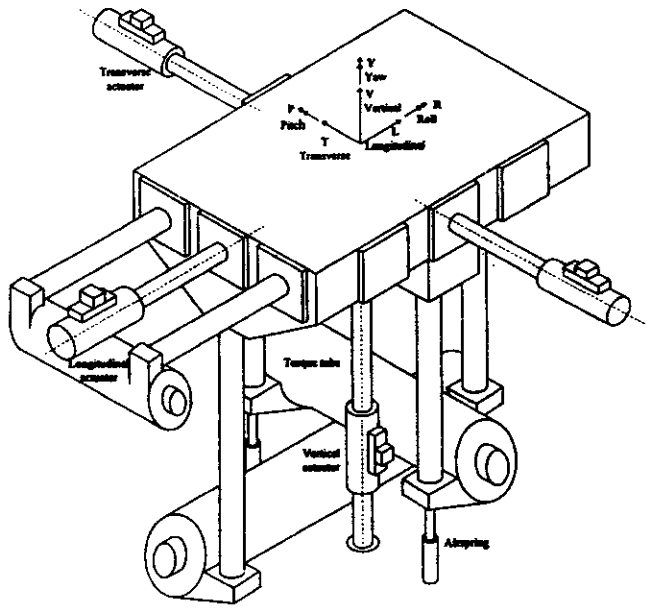

Fig. 1 General perspective of LNEC shaking table (Crewe, 1997)

Each system is composed of a torsionally very stiff torque tube (with a thickness of 2 cm and a diameter of 1.2 and 0.8 m for the case of horizontal and vertical tubes, respectively), which can rotate around its longitudinal axes and is supported at both ends by bearings. These tubes, connected to the table by means of vertical or horizontal rods, prevent significant overturning rotations at the table by providing a large reaction force to any pair of vertical or horizontal forces developed through table rotation. Nevertheless, minor flexibility is present, and overturning of the table can be observed, albeit to a relatively reduced extent. To correct such behaviour, the installation of short stroke actuators in the connecting rods, is being considered as a necessary upgrade for the near future (Crewe, 1997).

The steel platform measures 5.6×4.5 m^2 in plan, weighs 40 tonnes, and can carry a maximum payload of 40 tonnes. The platform is driven by one 1000 kN longitudinal, two 300 kN transverse and one 300 kN vertical servo-actuators, located on the centrelines of the table. The maximum acceleration input, under zero payload, is ±1.8g, ±1.1g and ±0.6g in the longitudinal, transverse and vertical directions, respectively. Peak velocity is ± 23 cm/s and maximum displacement is ±175 mm in all directions. The former limitation does impose an important restriction to the capacity of the table, since the use of accelerograms exhibiting much higher values of velocity is common. Hence, an upgrade to the hydraulic pumping station of the table, which will significantly increase the oil-flow capacity of the system, thus increasing its velocity limit, is currently being undertaken.

The shaking table is controlled by an INSTRON 8580 digital control system, with the control and matching software running on two independent computers. RSPlus provides control over the shaking table hardware and the SPiDAR matching software generates the signal forms required for the tests. Earthquake time histories are matched using a non real-time adaptive control algorithm, the full details of which are given elsewhere (Duque and Bairrao, 2000). The input and acquisition frequency used in the tests was 200 Hz. A more detailed and thorough account of the characteristics of this experimental facility can be found in the ECOEST/PREC8 report by Crewe (1997).

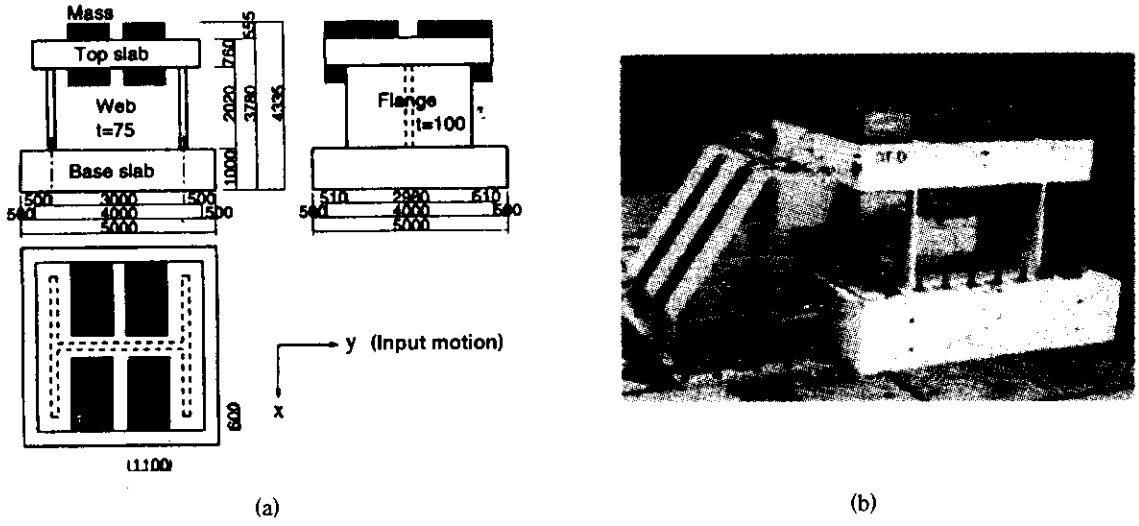

Fig. 2 Dynamic testing of RC walls using slab to support inertia mass :
(a) Inoue et al. (1997) (b) Yabana et al. (1996)

2. Inertia Mass

Due to the large scale nature of the specimens, equally large masses are needed to achieve the flexural capacity of the models. However, due to the dimensions of such mass blocks, it is not possible to simply rest these at the top of slender individual wall specimens, such as those used in this experimental programme. In fact, to avoid the risk of lateral instability of the model (which could lead to collapse of the whole test-rig, under the application of seismic excitation), alternative methods for supporting the masses and transmitting the inertia loads to the model are required, some of which are summarised below.

One possible methodology is to add two auxiliary walls to both ends of the wall element being tested, as indicated in Figure 2. A load-support slab can then be added at the top of the H-shaped specimen, where the inertia masses are then placed. Examples of the application of such type of scheme can be found in the work by Yabana et al. (1996) and Inoue et al. (1997), amongst others, where a series of dynamic testing on reinforced concrete wall models are reported. Evidently, the boundary conditions of the wall specimen are changed in this way, since a H-shaped, as opposed to a rectangular shaped element, is tested. This, however, may or may not be a disadvantage, depending on both the prototype being modelled (which may in fact be a H-type wall) and the objectives of the test.

Another possible alternative is to carry the inertia mass blocks by means of an external support system, such as stiff steel frames. This procedure has been employed by Elnashai et al. (1988) and Rothe and König (1988), amongst others, to undertake dynamic testing of reinforced concrete walls, and is shown schematically in Figures 3(a) and 3(b), respectively. Both systems have the advantage of allowing free translation and rotation in the direction of shaking, thus satisfying the isolated wall boundary conditions, whilst preventing any out-of-plane deformation. In addition, in the set-up shown in Figure 3(a), the inertia load is connected to the loading beam by means of shear links throughout its entire length, whilst in scheme depicted in Figure 3(b), a pinned connection at the centre of the loading beam is used to transmit the inertia load.

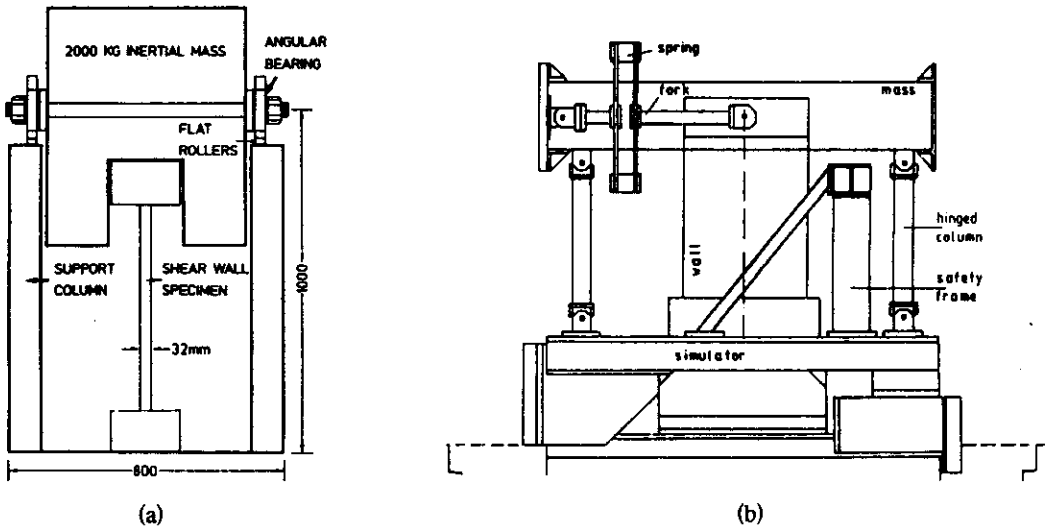

Fig. 3 Testing of RC walls using auxiliary frames to support inertia masses: (a) Elnashai et al. (1988) (b) Rothe and Konig (1988)

Some disturbance to the free-boundary condition at the top of the wall is introduced by both these schemes. In case (a), compression deformation is not allowed since the inertia mass cannot travel downwards, whilst in case (b), extension of the wall will also be slight restrained since the neutral axis depth is not located at the centre of the section (it continuously changes position according to the level of deformation imposed). In addition, case (b) features also a spring connection between the auxiliary frame elements and the mass (otherwise the whole assembly would be extremely stiff), which does introduce significant changes to the behaviour of the model. However, as mentioned earlier, if the objective of the tests is not to reproduce with exactitude the response of a particular prototype, then such discrepancies may not constitute a major drawback. That seemed to be the case in both these applications.

A third solution to the problem of transmitting large inertia loads to slender wall specimens has been tried out by Pavese et al. (1999). In this case, a L-shaped mass-carrying system that is allowed to slide on a fixed supporting structure, located outside the shaking table, is used to carry the mass blocks. The L-shaped assembly is linked to a ring, at the top of the model, by means of a steel rod, as shown in Figure 4. The latter is connected to the ring and L-shaped structure through spherical swivels, thus allowing free rotations. With such scheme, the weight and overturning moment transmitted to the table are significantly reduced, enabling easier control over both the input and output of the test (Bairrao and Vaz, 2000).

This scheme presents also a high degree of flexibility in terms of assembly and disassembly of the test-rig (a number of test runs on different specimens are usually required) since release of the pin between the connecting rod and the steel collar is all that is required to disconnect the model from the loading mechanism. Further, its application to other experimental programmes, where distinct specimens are used, is also relatively straightforward, since the height of the connecting rod can be easily adjusted according to the characteristics of the models, the mass blocks are easily removed or added to the load-carrying rig, and the bolted steel collar configuration can also be changed to different shapes and sizes without difficulties.

Finally, both types of mass-supporting schemes shown in Figures 3 and 4 present the advantage of allowing the use of large masses without introducing changes in the response characteristics of the model (since the mass blocks are not supported by the models). Such feature is often required for full satisfaction of similitude laws, as discussed in subsequent sections.

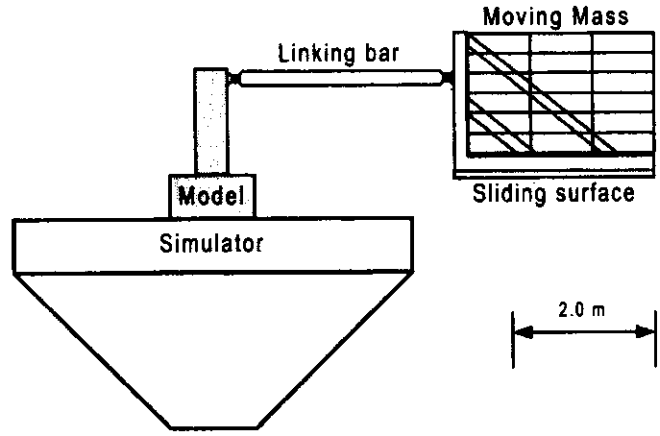

Fig. 4 Testing of RC piers using external support for inertia masses (Pavese et al., 1999; Bairrao and Vaz, 2000)

For the purpose of the current work, and due to the low velocity capacity of the shaking table, a very large inertia mass (20 tonnes) was required to achieve the flexural capacity of the models. At LNEC, the test-rig shown in Figure 4 was readily available, since this had been used in a previous experimental programme (Pavese et al., 1999). Therefore, its adoption to the present work was evidently advantageous, in terms of acquired experience in its use, as well as reduction of costs. In addition, the drawbacks associated to such scheme, namely the high friction at the sliding bearing and the need for an additional out-of-plane restraining mechanism, considered below, did not constitute a major impediment to the objectives of the experimental programme, as discussed in subsequent sections. Therefore, the test-rig shown in Figures 5 and 6 was adopted.

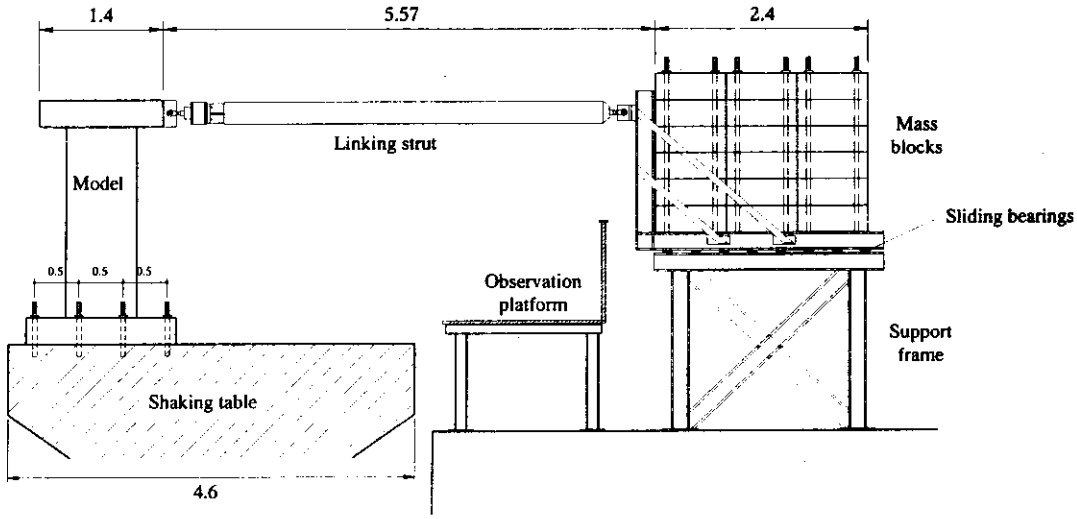

Fig. 5 Schematic representation of test set-up

Fig. 6 Test set-up

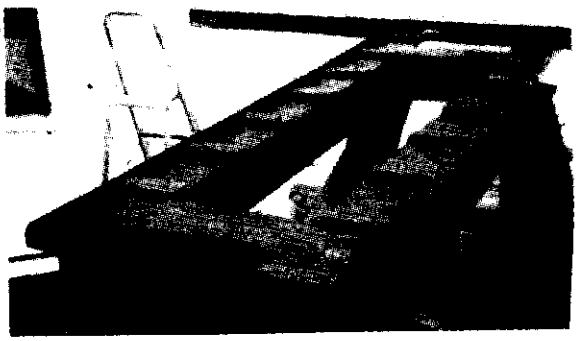

Fig. 7 Sliding bearings

3. Sliding Bearings

The adopted mass-supporting system requires a low-friction sliding surface between the L-shaped structure and the fixed support. This can be achieved by the use of a system of either rollers or sliding bearings. For the purpose of this work, the latter solution was employed, as shown in Figure 7, making use of Teflon pads coated with a lubricant.

Prior to each test, a low frequency $(T = 2\,\mathrm{s})$ sine curve and a ramp signals, depicted in Figure 8, were applied to the platform. Such input motions, applied at relatively low velocity, induced negligible response of the models. Therefore, any source of resistance to the applied motion could originate only from friction being developed between the pads and the L-shaped assembly. In this manner, the level of friction could be quantified.

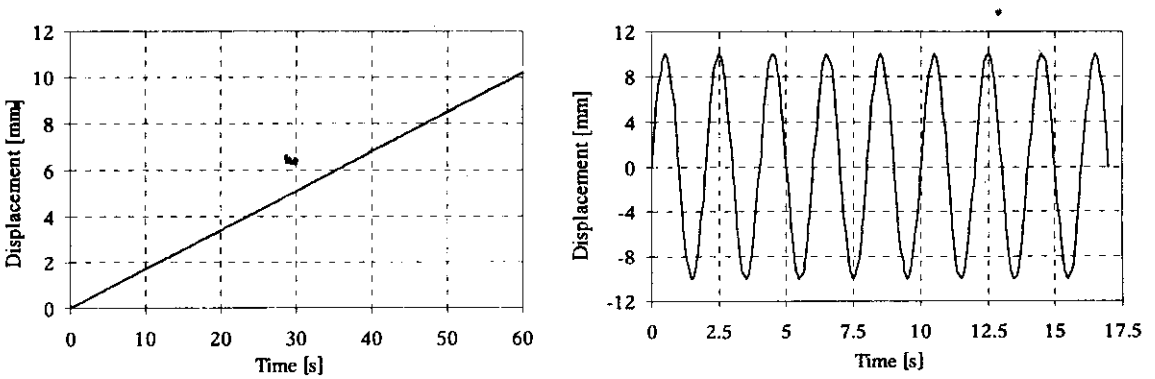

Fig. 8 Ramp and sine signals employed for the quantification of friction level

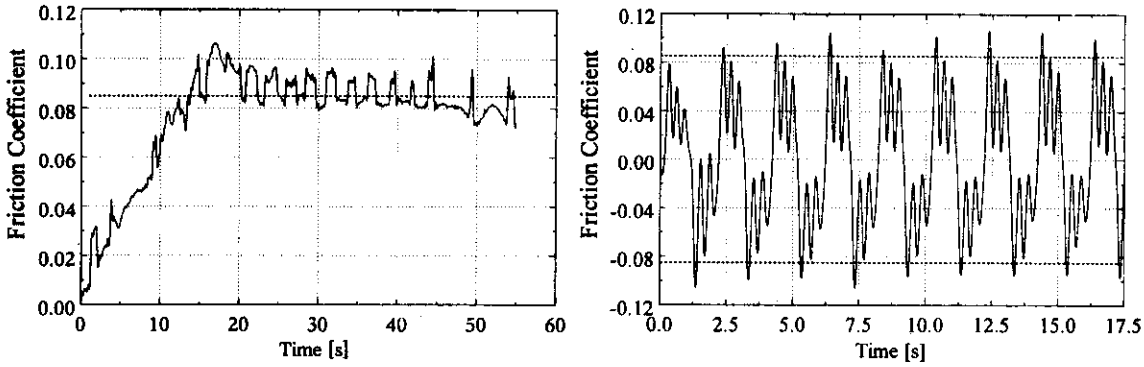

Fig. 9 Determination of level of friction

Ideally, the level of friction between the pads and the mass-carrying system should be very close to zero. However, this was, unfortunately, not the case. As it is observed in Figure 9, the level of friction is relatively high at a value of 8.5%, thus introducing strong damping in the response of the models. Further, the sliding system does not allow for a smooth response of the models, as observed in Figure 9 where shorter frequency vibrations, not present in the input motion and not caused by vibration of the models, are visible.

The main disadvantage associated to such damping is the resulting smaller dynamic amplification factor, which in turn reduces the seismic demand on the models. In addition, natural period of vibration of the models, prior to and after each test, cannot be estimated using hammer testing (or similar methods), since any small motion imposed on the model is damped to zero almost instantaneously. In fact, the critical damping coefficient ξ, usually adopted with a value of 0.05 for reinforced concrete structures, was estimated in this case to be twice such figure.

For the purpose of the current work, however, such drawbacks did not constitute causes of particular concern since, as mentioned earlier, the objectives were the assessment of retrofitting techniques, rather than the accurate reproduction of real response of a particular prototype. Nevertheless, it is clear that such sliding mechanism does not provide an ideal solution, and it is the opinion of the author that the use of roller bearings provides a more adequate alternative.

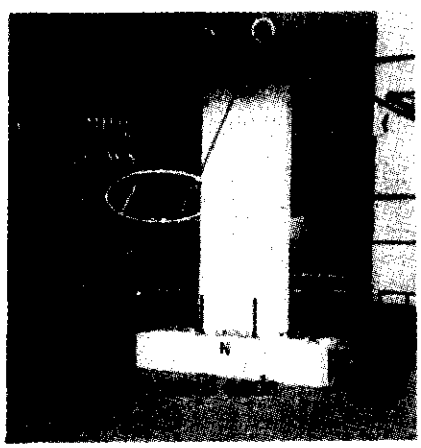

Fig. 10 Out-of-plane restraining device

4. Out-of-Plane Restraining Device

As mentioned earlier, the adopted test-rig configuration had been previously applied in an experimental programme at LNEC that preceded the current work. However, such programme consisted of a series of tests on hollow bridge piers, with a predominantly square section, which did not pose any problems of out-of-plane deformability. This, however, was not the case for the models being studied

under the current programme, which, due to their high length-to-width ratio (8/1.2), did show excessive flexibility in the plane perpendicular to the input motion.

An initial test, carried out on a model without any type of out-of-plane restrain, clearly confirmed this problem since the transverse displacements at the end of such experiment reached values as high as 60 mm (2.8% drift), even though no input movement in such direction was detected in the platform. Therefore, an out-of-plane restraining mechanism, consisting of the use of four inclined bars pinned to the model as shown in Figure 10, was introduced to prevent deformation in the transverse direction of the model.

In Figure 11, the out-of-plane deformations of two models with and without the transverse restraining mechanism, specimens SW3 and SW2, respectively, are shown. The efficacy of the adopted solution is clear since the deformation measured in model SW3 is practically negligible.

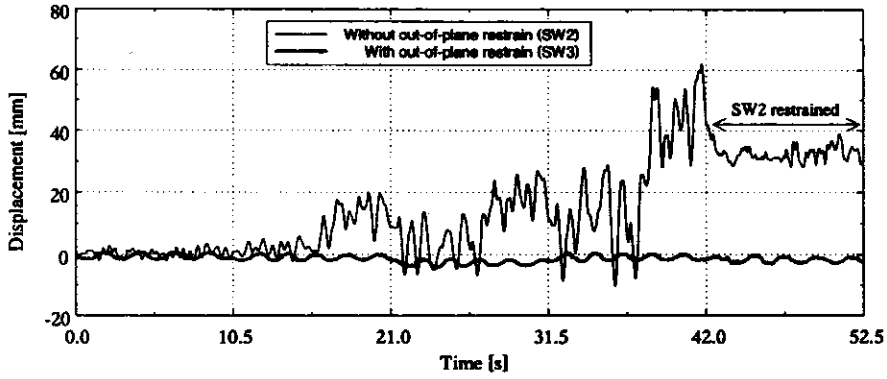

Fig. 11 Out-of-plane displacement in models SW2 and SW3

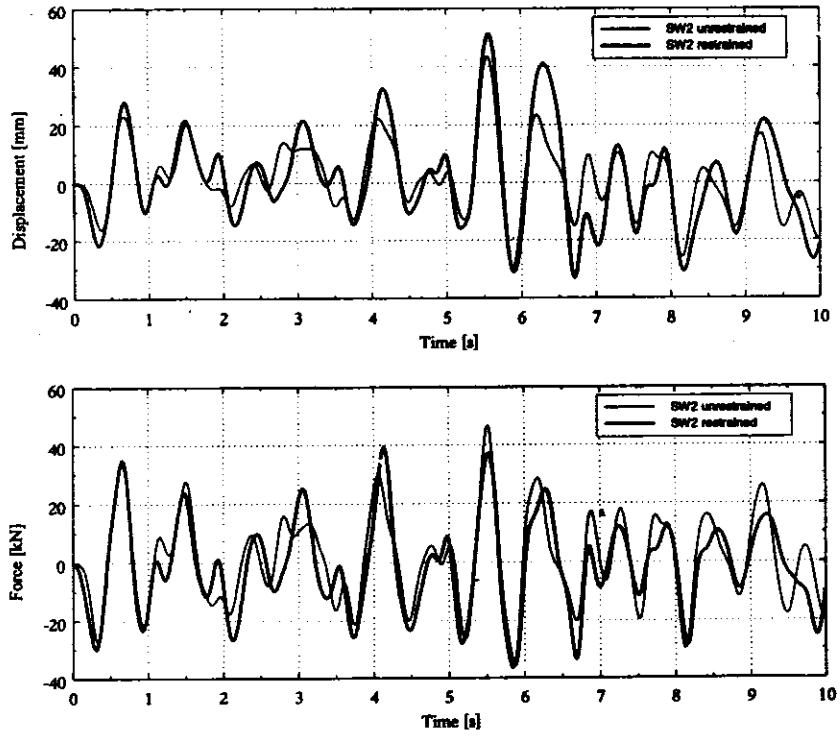

Fig. 12 Effect of out-of-plane restraining mechanism on model SW2

Further, which in order to assess the effect that the guiding mechanism has on the in-plane response of the structure, noting that some restraint is introduced to vertical extension of the wall, model SW2 was re-tested with the mechanism attached. Comparison between the response displacement and horizontal force time-histories, before and after restraining, show only minor differences (Figure 12), with the re-tested model showing slightly higher levels of deformation, as would be expected due to damage accumulation. Therefore, it can be concluded that the out-of-plane restraining scheme does not introduce noticeable changes to the response of the models, whilst controlling transverse deformation.

5. Instrumentation

A relatively light instrumentation plan, consisting of 11 transducers, six optical readers, four accelerometers and one cell-force, was utilized in this work, due to time and financial constraints. This prevented, for instance, strain gauging of reinforcement bars, which are usually most useful in providing important information regarding the different performance levels of the models: point of first yield, attainment of failure strain level, plastic hinge length, and so on. Nevertheless, since the objectives of the experimental programme focused on assessment of the effect of the proposed selective techniques on the global behaviour of the models, such level of instrumentation detail was deemed as non-vital. In addition, the layout of the 22 instruments utilized, shown in (see Figure 13) was carefully planned so as to maximize the amount of information to be retrieved and post-processed, as shown in subsequent sections.

At the foundation beam, three transducers (two verticals and one horizontal) were used to measure displacements at the base of the model so as to check that this is properly fixed to the platform (confirmed by the practically nil values measured at these locations). In the wall, four vertical transducers were located on each side to measure vertical displacements, which were then used to derive rotation/curvature profiles and to determine the flexural component of the model's deformation. Five optical readers located at the centre of the wall, and distributed throughout its height, were used to measure horizontal displacements. It is important to notice that the distribution of the instruments throughout the height (Figure 13) reflects the need for refinement near the base of the specimen where inelasticity was expected to occur.

The transverse (out-of-plane) displacement of the model was measured by an optical reader located on one side of the model. A force cell was located in the mass/model connecting rod to measure the inertia load acting on the model, and the response acceleration at the top of the model was measured by an accelerometer located in the loading beam. In the platform itself, two accelerometers were attached to record accelerations in both directions, and were used to check the accuracy of the input signal.

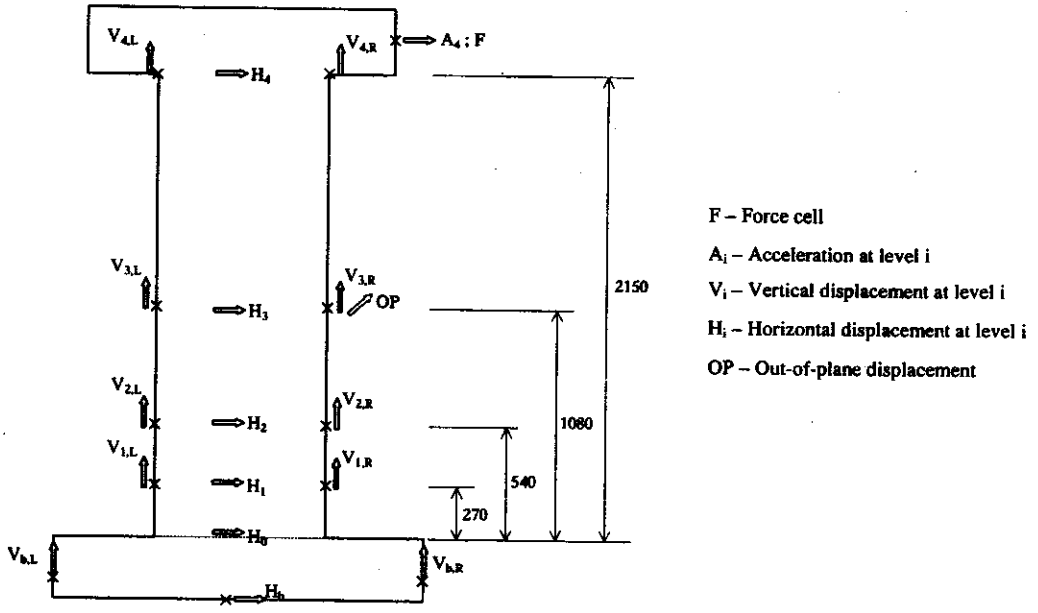

Fig. 13 Instrumentation plan

DESIGN OF THE MODELS

1. Similitude Laws

The need for reduced scales in shaking table testing, as discussed earlier, raises a number of similitude difficulties (Okada, 1978). In the case of reinforced concrete models, full reproduction of the true dynamic response of the prototype requires accurate simulation of geometry, initial and boundary conditions, stress-strain relationship of the materials and mass and gravity forces. Geometric similitude is achieved by a direct application of a geometric scaling factor, leading to the construction of small specimens, which may or may not present difficulties, depending on how small the adopted scaling is (Carvalho, 1998).

Regarding the initial and boundary conditions, the main difficulties arise only in the case where modelling of soil-structure interaction is also sought. Presently, attempts at solving these problems are being made (e.g., Konagai and Nogami, 1997; Ahsan et al., 2000), involving concepts of sub-structuring where part of the specimen is physically modelled and tested on the shaking table, and another part is numerically represented and analysed. The experimental and analytical responses of each 'part', at each time-step, are then considered in the calculation of the input motion for the subsequent time-step. It is noteworthy that such testing methodology requires real-time control of shaking tables, a feature not yet adopted as standard in a large number of experimental facilities.

The accurate simulation of the stress-strain relationships poses a more challenging problem, as discussed by Bedell and Abrams (1983), since small scale modelling normally calls for the use of micro-concrete and specially manufactured reinforcement bars. These should exhibit the same type of behaviour as of 'standard' materials, throughout the complete range of strains and stresses experienced in the test. For the case of concrete, the accurate simulation of its compressive and tensile strengths together with ultimate strains is critical. As far as the reinforcement material is concerned, the yield stress, strain hardening and uniform elongation are the main parameters requiring correct simulation. Finally, the bond between these two materials must also be accurately reproduced, as reported by Carvalho (1998).

The simulation of mass and gravity forces is closely linked to the similitude laws adopted. In dynamic testing of scaled models, the Cauchy and Froude laws must usually be respected. The former is adequate for phenomena in which the restoring forces are derived from stress-strain constitutive relationships, whilst the latter applies to cases where gravity forces are important. It is thus clear that for the realistic modelling of non-linear dynamic response of structures, both similitude laws must be respected; although, in practical applications, this is not always feasible, and some distortion, usually between the force and weight scales, is allowed for (Carvalho, 1998).

Table 1: Scale Factors for the Satisfaction of the Cauchy and Froude Similitude Laws (Carvalho, 1998)

Parameter	Symbol	Scale Factor (Cauchy)	Scale factor (Cauchy+Froude)
Length	L	$L_P/L_M=\lambda$	$L_P/L_M=\lambda$
Modulus of elasticity	E	$E_P/E_M=e=1$	$E_P/E_M=e=1$
Specific mass	ρ	$\rho_P/\rho_M=\rho=1$	$\rho_P/\rho_M=\rho=\lambda^{-1}$
Area	A	λ^2	λ^2
Volume	V	λ^3	λ^3
Mass	m	λ^3	λ^2
Displacement	d	λ	λ
Velocity	v	1	$\lambda^{1/2}$
Acceleration	a	λ^{-1}	1
Weight	w	λ^3	λ^2
Force	F	λ^2	λ^2
Moment	M	λ^3	λ^3
Stress	σ	1	1
Strain	ε	1	1
Time	t	λ	$\lambda^{1/2}$
Frequency	f	λ^{-1}	$\lambda^{-1/2}$

The simultaneous satisfaction of the Cauchy and Froude similitude laws, assuming that the prototype and model materials are the same $(E_P/E_M = 1)$, leads to the scale factors presented in Table 1. Here the scale factors for the simpler case of respecting the Cauchy law alone are also given. It is noteworthy that consideration of the Froude similitude requires a significant increase of the specific mass in the model since ρ becomes inversely proportional to the geometric scale factor λ. This presents difficulties in terms of either finding non-standard higher density materials, or adding mass to the model without influencing its stiffness, since the increase of mass rises very sharply as the size of the model is reduced (e.g., in a model built at 1:5 scale, the mass to be added represents 80% of the total mass of the model (Carvalho, 1998)). For these reasons, it is not uncommon for the scal of the specific mass to be considered independently of the geometric scale, as mentioned above.

2. Prototype and Model Design

As stated earlier, the current experimental programme did not attempt to reproduce any particular real scenario involving a real structure (or type of structure) subjected to a real earthquake input motion (or set of input motions). The main objective was rather to assess the effectiveness of innovative retrofitting techniques under dynamic load conditions. Therefore, full satisfaction of the two similitude laws described above was not required.

Nevertheless, the models employed in the tests did try to represent a typical prototype structure, considered in this application as being the case of slender structural walls used in many reinforced concrete buildings, as examplified in Figure 14. The prototype considered was a 3.2 m high wall by 1.2 m wide. As indicated in Figure 14, only the critical region of the multi-storey wall (adopted here as the first storey) was considered as the prototype. The models may also be representative of larger and taller walls (assuming higher geometric scale factor) in cases where a cantilever response mode is clearly dominant.

In order to attain damage in the models with minimum demand on shaking table input, ductility class "L" (as defined in Eurocode 8 (CEN, 1996)) was adopted to determine section size and longitudinal reinforcement requirements. By following such prerequisites, a wall element with a thickness of 200 mm and the height and width indicated in Figure 14 was obtained. The boundary elements in the prototype were 200×250 mm^2 and the reinforcement in these areas was chosen following the code minimum reinforcement ratio of 0.5%, yielding four 12 mm bars in each end. In terms of confinement, 6 mm diameter hoops spaced at 70 mm centres in the lower half of the model and at 150 mm in the upper half, were designed.

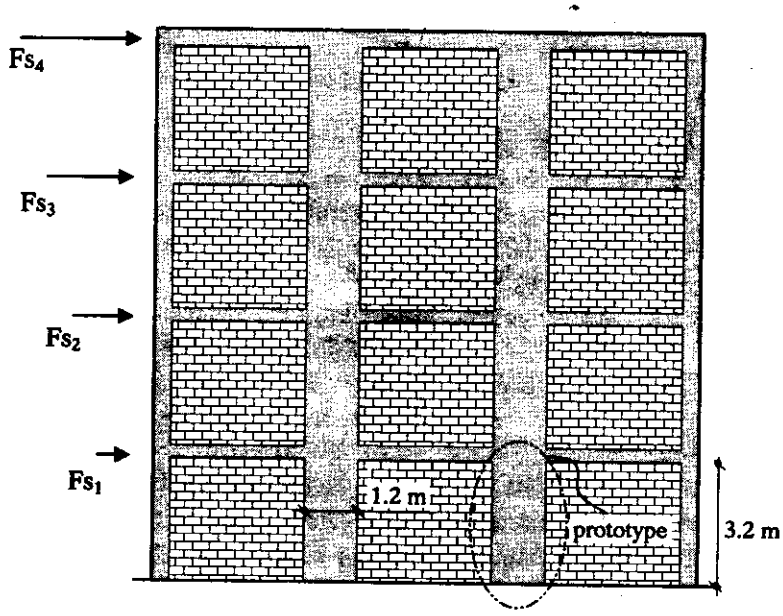

Fig. 14 Prototype building with slender structural walls

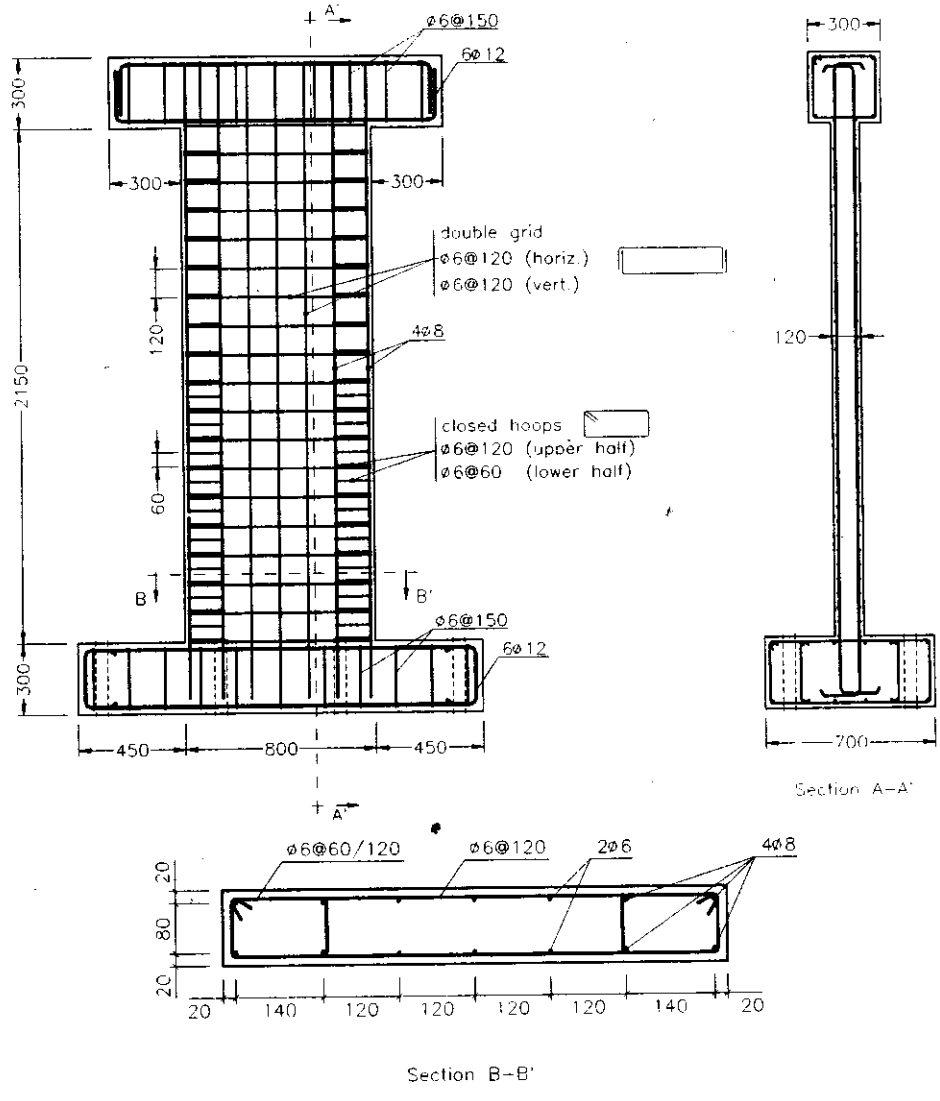

Fig. 15 Dimensions and detailing of test specimens

Regarding shear design, since the objective of the tests was to analyze the response of the models in flexure, the prototype was designed using EC8 Class "H" rules for shear detailing. Thus, both vertical and horizontal reinforcements in the web followed the minimum requirements for this class in terms of area and spacing, to safeguard against shear failure, thus resulting in 10 mm bars at 175 mm centres.

A geometric factor of 1.5 was then applied to scale down the dimensions and reinforcement detailing of the prototype, resulting in a model with the characteristics shown in Figure 15. This model was then checked against shear mode failure using capacity design principles and following guidelines prescribed in EC8 for such verifications.

The employment of large-scale models enabled the use of normal concrete and reinforcement bars with no need for any special provisions. Thus, the concrete specified was C20/25 $\left(f_k = 20\,\text{MPa}\right)$, representative of older design structures requiring strengthening, and the reinforcement steel was Class S400 $\left(f_{yk} = 400\,\text{MPa}\right)$. Note that the nomenclature and material classification being used follows the conventions defined in Eurocode 2 (CEN, 1991).

The dimensions of the loading beam were defined in accordance with the characteristics of the load-transfer mechanism, resulting in a cross-sectional area of 300×300 mm^2. Minimum reinforcement

detailing, for construction purposes only, was adopted here. As for the foundation, its length and width were determined to allow the use of eight fixing points to the table, where the existing grid is $0.5 \times 0.5\ m^2$. The height of the foundation was determined to provide sufficient protection against punching shear failure.

The flexural reinforcement of the foundation was designed using an estimated overturning moment of 220 kN-m, corresponding to a horizontal force of approximately 100 kN at the top of the model. This level of horizontal load corresponded to the expected capacity of the model repaired with reinforced concrete jacketing, which was anticipated to be the strongest model used in the tests (Pinho et al., 2000).

Finally, it is worth noting that, for simplification, no additional axial load was applied to these models, in addition to the weight of the loading beam and connecting steel collar. Such parameter does not affect the effectiveness of the retrofitting schemes being tested in this programme; thus, introduction of axial load in the model was not considered as a fundamental requirement.

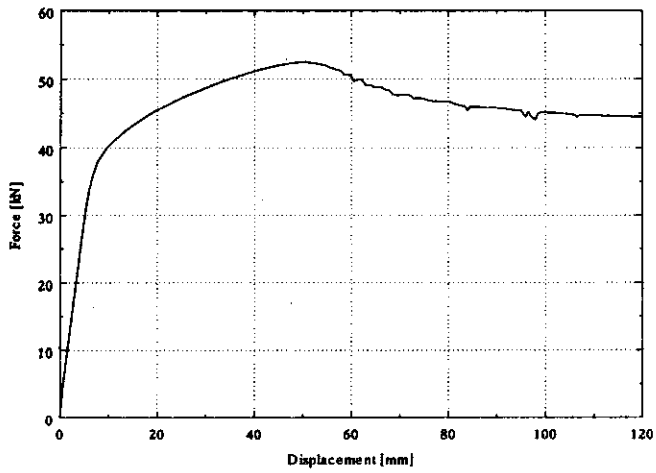

Fig. 16 Analytical monotonic response of intact model

3. Estimation of Flexural Capacity and Definition of Inertia Mass

In order to define the level of acceleration input and inertia mass required, the flexural capacity of the specimens needed to be determined first. The capacity of the model was evaluated using the finite element (FE) program ADAPTIC (Izzuddin and Elnashai, 1989).

In Figure 16, the results from a simple monotonic analysis indicate that the expected flexural capacity of the specimens is 53 kN. Since selective strengthening of the models targeted an increase of 25% in flexural capacity (Pinho et al., 2000), the required maximum equivalent horizontal force at the top of the model was assumed to be approximately 66 kN (excluding the case of the jacketed model).

Due to the expected high friction levels between the Teflon pads and the inertia mass, a dynamic amplification factor of 1.8 was assumed at this stage, corresponding to equivalent viscous damping of 10% (such assumption was later confirmed to be acceptable since test results showed the dynamic amplification factor to vary between 1.5 and 2.0).

Also, the maximum input acceleration that the table is capable of producing by using the artificial accelerogram chosen for the tests was 0.18g, as indicated below. Therefore, in order to achieve the target force of 66 kN, the inertia mass required was 20 tonnes.

Finally, the model repaired with reinforced concrete jacketing was expected to possess a flexural capacity of 100 kN. Therefore, and since it was not possible to achieve such levels of demand within the present experimental set-up, it was envisaged that the dynamic testing of this model would be followed by monotonic loading in order to take the specimen to collapse and assess its full capacity.

4. Design of Retrofitted Models

Eleven tests on eight models were envisaged. Three of the models were tested twice, being firstly tested as bare intact specimens and then re-tested after being repaired. In this manner, the response characteristics of intact specimens, necessary for comparison with retrofitted models behaviour, would be appraised. The remaining five models were upgraded before being tested up to collapse. In Table 2, a summary of the testing programme is included.

Table 2: Summary of Testing Programme

Ref.	Description	Objective of the test
SW1	unconfined intact wall	damage specimen (stiffness/strength deterioration)
SW1R	wall repaired by jacketing	evaluate effects of jacketing on wall behaviour
SW2	confined intact wall	damage specimen (stiffness deterioration)
SW3	confined intact wall	damage specimen (stiffness deterioration)
SW3R	wall repaired with EBSP[1]	fully recover original stiffness
SW4	wall retrofitted with EBSP	controlled increase in stiffness of wall
SW5	wall retrofitted with EURB[2]	controlled increase in strength of wall
SW6	wall retrofitted with ECSP[3]	controlled increase in ductility of wall
SW6R	wall repaired by epoxy injection	evaluate level of stiffness reinstatement
SW7	wall retrofitted with EURB and ECSP	increase both strength and ductility
SW8	wall retrofitted with EBSP and ECSP	increase both stiffness and ductility

[1] EBSP – External Bonded Steel Plates

[2] EURB – External Unbonded Reinforcement Bars

[3] ECSP – External Confinement Steel Plates

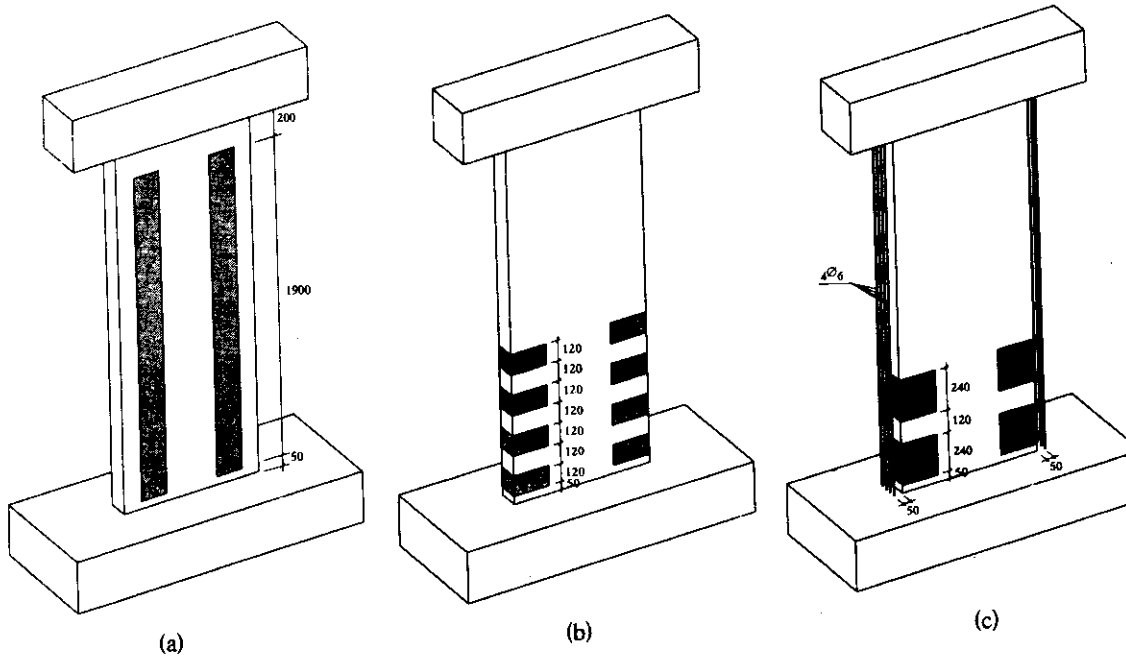

Fig. 17 Selectively retrofitted models: (a) SW4 (b) SW6 (c) SW7

Selective retrofitting techniques were applied to six specimens, covering the cases of stiffness-only, strength-only and ductility-only interventions (Pinho et al., 2000). In models SW4 and SW3R, stiffness-only intervention was applied as both an upgrading and a repair technique, respectively. Regarding strength-only intervention, two tests were envisaged (SW5 and SW7), with similar external reinforcement

detailing but different values for the design slackness of the external re-bars. Finally, regarding ductility-only intervention, three tests were envisaged using intact models without internal ductility detailing (SW6, SW7 and SW8). In Figure 17, the selective schemes adopted in three of the wall models are schematically illustrated (detailed description of the applied schemes, and their underlying principles, can be found in the work by Elnashai and Pinho (1998)).

Furthermore, two of the most popular repair and/or strengthening techniques, reinforced concrete jacketing and epoxy-resin injection, were also tested in the current research programme. Reinforced concrete jacketing was applied in model SW1R, which had been previously damaged. Epoxy resin injection was applied to model SW6R. The latter suffered some damage during its first test run, but did not reach collapse; hence, stiffness degradation occurred without substantial loss of strength.

Table 3: Summary of Concrete Characteristics

Model	Average compressive strength (MPa)
SW1	25.4
SW2	21.6
SW3	24.6
SW4	24.8
SW5	27.5
SW6	33.5
SW7	30.0
SW8	25.7

CONSTRUCTION OF MODELS

The models were built by a private contractor, sub-contracted by LNEC for this task. The concrete, however, was produced at the concrete laboratories at LNEC. Five test cubes were produced for uniaxial compression testing, two of which were tested after 7 days of cure, whilst the other three were tested after 28 days. In Table 3, a summary of the average compressive strength is given. With the exception of SW2, the results are generally satisfactory with values within the limits expected for the specified C20/C25 concrete.

Table 1: Properties of Steel

	f_y (MPa)	f_t (MPa)	f_y/f_t
Min	473	547	1.07
Max	554	594	1.17
Mean	501	567	1.13
Std. Dev.	25	13	0.03

With regard to the properties of the reinforcement steel, specified as S400, a relatively comprehensive set of results is also available. Eleven steel bars, similar to those used to construct the models, were tested at LNEC, providing stress-strain relationship curves, as well as a table of results. In Figure 18, the typical stress-strain diagram is shown. In Table 4, maximum, minimum and mean values for yield (f_y) and ultimate (f_t) stresses are given, together with the ratio f_y/f_t. The values observed are typical of Tempcore steel, the most common commercially available steel in Portugal, and therefore correspond to what was expected.

Unfortunately, this type of steel is characterised by low values of hardening ratios f_y/f_t, with obvious unfavourable effects on the available ductility of the test specimens. In fact, for the studied sample (which is clearly not sufficiently large to grant full statistical validity), the mean hardening ratio of

1.13 does not even meet EC8 requirements for Medium Ductility Class structures, which serves as an indication that lower ductility than initially envisaged was to be expected from the models.

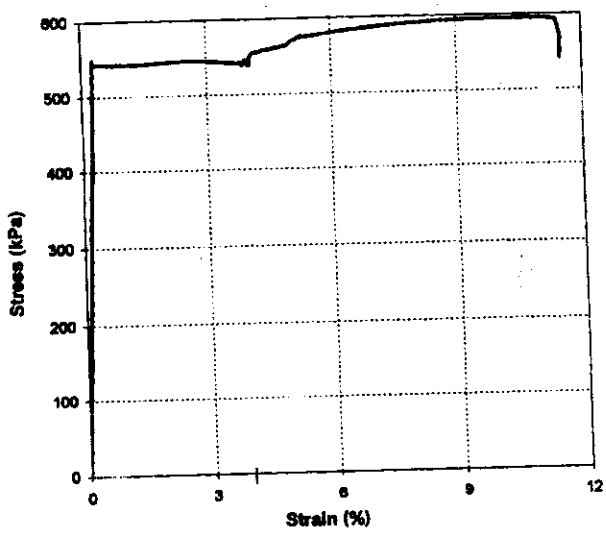

Fig. 18 Typical stress-strain relationship of steel used in the tests

Finally, it is noteworthy that details of the application of the repair and strengthening schemes, together with a thorough account of the design processes as briefly described above, is available in the work by Pinho et al. (2000).

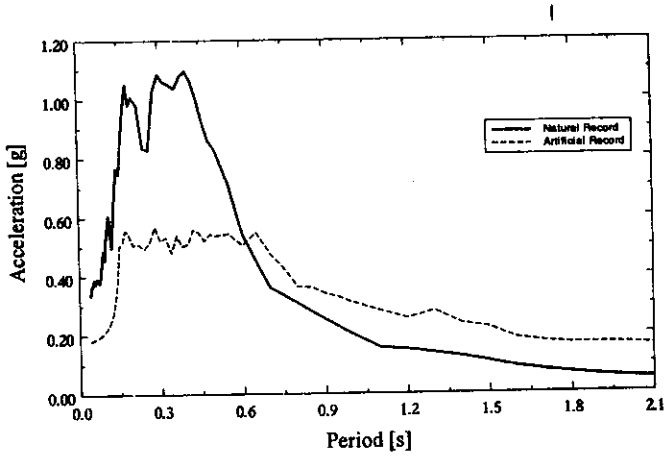

Fig. 19 Response spectrum of artificial and natural (Emeryville, 1989) records

INPUT MOTION

As mentioned earlier, since full implementation of similitude laws was not sought, the velocity and time scale factors specified in Table 1 were not considered, and thus no changes in duration and frequency content of the records were applied. It is also important to notice that, in order to maximize the amount of information extracted from the testing of each specimen, an appropriate selection of the testing sequence is required. In the present work, identification of a number of response parameters of the models was needed: initial stiffness, point of yield, maximum flexural strength and deformation capacity. Therefore, the models were tested under progressively more severe earthquake actions (scaled up considering the value of peak acceleration as the reference factor).

Due to the characteristics of the shaking table, as described earlier, and its interaction with the models, a combination of artificial (AR) and natural records (NR) was found, through preliminary analytical studies, to be of most use to achieve the objectives of the tests. Both records possessed response spectra with corner periods enclosing the range of possible periods of vibration of the model (0.2-0.6 s), thus guaranteeing maximum amplification of motion as the period of vibration of the models elongates during testing. The spectra are shown in Figure 19 for 5% viscous damping.

The natural record, consisting of the accelerogram recorded at the Emeryville station during the Loma Prieta earthquake of 1989 (United States), possesses higher maximum input acceleration and therefore shows higher values of response acceleration (Figure 19). However, the artificial record is characterised by an equally 'artificially' rich frequency content, with a high number of peaks throughout its intended frequency range (Figure 20(a)), thus resulting in higher energy content. On the other hand, the natural record possesses fewer but stronger pulses as shown in Figure 20(b) and consequently, both records reveal similar peak velocities, as shown in Figure 21, close to the limit of the shaking table capacity (23 cm/s).

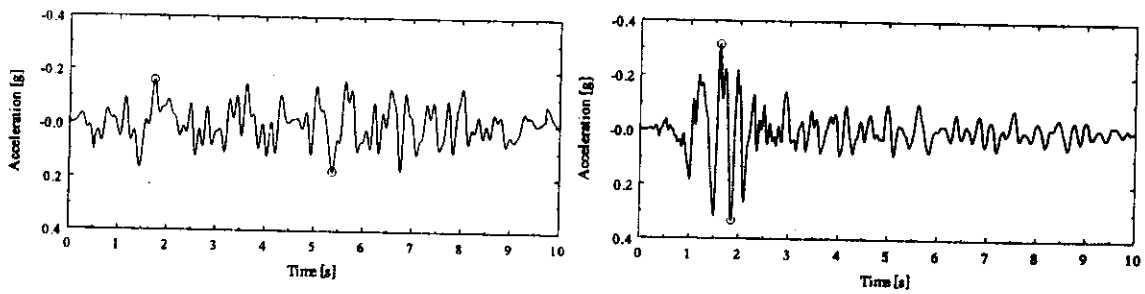

Fig. 20 Acceleration time-history for (a) artificial record (b) natural record

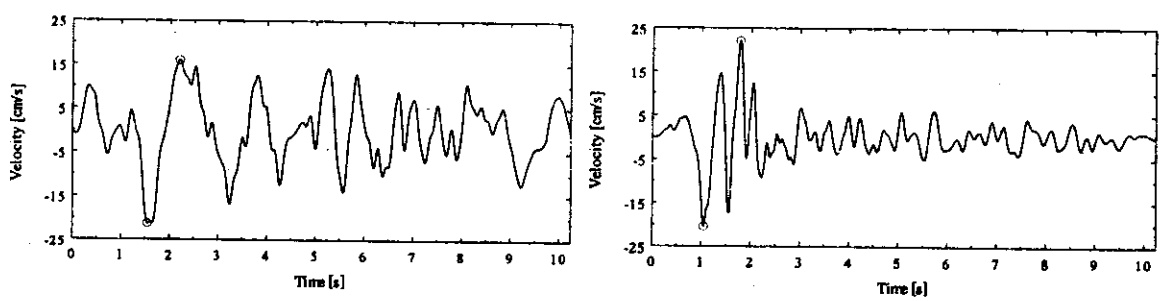

Fig. 21 Velocity time-history for (a) artificial record (b) natural record

In Table 5, the sequence of input motion used in each test is described. All tests started with a sine-curve (SN) or ramp (RP) signals. As mentioned earlier, these were used in the beginning of each test to evaluate the level of friction between the mass blocks and the sliding bearings, and to assess any eventual material deterioration of the Teflon pads. The numeral at the right of the nomenclature indicates period for the case of the sine input, or peak displacement in the case of the ramp signal.

As mentioned above, and in order to guarantee a progressive damage to the models, the input motion was applied split into several stages, while using scaled up or scaled down accelerograms. In addition, and in some cases, accelerograms were used in succession, without pause, mixing both natural and artificial records. Therefore, as shown in Table 5, a mixture of both records was utilised providing a combination of isolated strong pulses from the natural record with the "weaker" but more frequency-intensive artificial input motion. Here, the numeral by the side of the nomenclature (AR or NR) indicates the maximum input acceleration of each record.

Table 1: Testing Stages for Each Model

Model	Stage 0	Stage 1	Stage 2	Stage 3	Stage 4	Stage 5	Stage 6
SW1	SN_2 SN_1	AR_0.14	NR_0.25	NR_0.33	AR_0.18		-
SW1R	SN_2	AR_0.14 AR_0.14	NR_0.25 AR_0.14	AR_0.18 AR_0.18	NR_0.41 AR_0.22	MONOT	-
SW2†	RP_18	AR_0.09	AR_0.14	AR_0.14	AR_0.18	AR_0.22	-
SW3	RP_10 SN_2	AR_0.05	NR_0.17	NR_0.17	NR_0.25	NR_0.33	AR_0.18
SW3R	SN_2	AR_0.14 AR_0.14	NR_0.25 AR_0.14	AR_0.18 AR_0.18	NR_0.41 AR_0.22	-	-
SW4	SN_2	AR_0.14 AR_0.14	NR_0.25 AR_0.14	AR_0.18 AR_0.18	NR_0.41 AR_0.22	-	-
SW5	SN_2	AR_0.14 AR_0.14	NR_0.25 AR_0.14	AR_0.18 AR_0.18	NR_0.41 AR_0.22		-
SW6	SN_2	AR_0.14 AR_0.14	NR_0.25 AR_0.14	AR_0.18 AR_0.18	-	-	-
SW6R	SN_2	AR_0.14 AR_0.14	NR_0.25 AR_0.14	AR_0.18 AR_0.18	-	-	-
SW7	SN_2	AR_0.14 AR_0.14	NR_0.25 AR_0.14	AR_0.18 AR_0.18	MONOT	-	-
SW8	SN_2 SN_2	AR_0.14 AR_0.14	NR_0.25 AR_0.14	AR_0.18 AR_0.18	NR_0.41 AR_0.22	-	-

† Out-of-plane mechanism added only in last stage

In Figure 22, the target input motion is compared with the acquired time-history at the end of a test. There is good agreement between the target and acquired motions (with the exception of the initial and final instants when the motion is applied gradually from/to resting position), thus indicating adequate control on table input. It is noteworthy, however, that such good agreement between the target and acquired input motions is of relatively little relevance for the present work, since the exact reproduction of a particular earthquake scenario was not sought. Nevertheless, it serves to illustrate that the application of the large inertia mass outside the table, which in turn reduces considerably overturning actions imposed on the platform, does reduce difficulties in shaking-table control, as previously discussed.

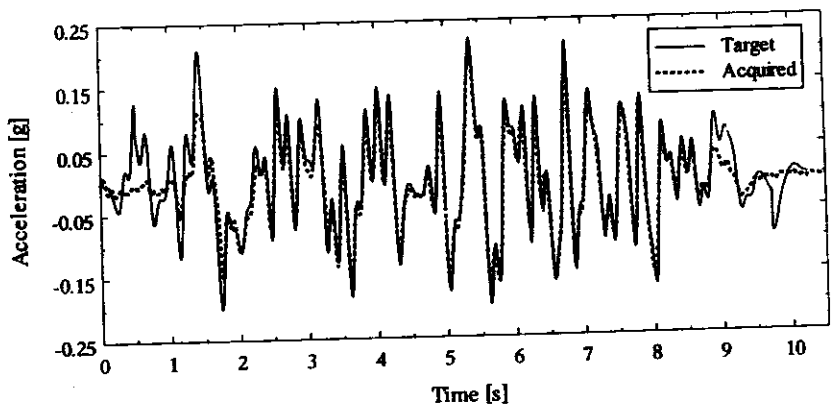

Fig. 22 Target and acquired input motion

POST-PROCESSING OF RESULTS

All data processing was performed by using Mathcad (Mathsoft, 1998), which is a numerical/mathematical tool for engineering applications. Several spreadsheets were created to read and post-process the raw data collected during the experiments, by using either built-in or user-programmed functions. Below, the collection of result plots created for each model at every stage is described and illustrative examples are included.

1. Digital Filtering

All data acquired during the tests was recorded in a simple text-format file for further processing. This data corresponded to the values read from the transducers and optical readers, and had not been manipulated in any fashion. It was therefore necessary that the results were filtered so that high-frequency vibration, associated to parasitic vibrations in the table and electromagnetic interference, could be removed from the results.

Generally, acquisition of data was carried out throughout a period of 30 seconds, which was sufficient to contain the 20 seconds input motion. The frequency of acquisition was 200 Hz $(\Delta t = 0.005\,\mathrm{s})$, resulting in an output of 6000 points.

A low-pass digital finite impulse response (FIR) filter was utilised to carry out filtering in time domain, as opposed to frequency domain. Such methods are quite efficient in filtering transient signals (not always well characterised by frequency-domain filters) and in speeding up the filtering process, since no Fourier transformations are required. The tapered window function, required to ensure that the filter has a finite order, was of the Hamming type, guaranteeing good stop-band attenuation. The length of the filter was set-up to 10% of the total number of points of the sample, thus ensuring a narrow transition band (sharp cut-off).

Taking into account that the elastic period of vibration of the intact model was 0.22 s, and since no important contribution from higher modes was expected, the pass-band frequency was chosen as 5 Hz $(T = 0.2\,\mathrm{s})$ Several sensitivity studies were also carried out in order to ensure that the choice of such value did not affect the response of the models.

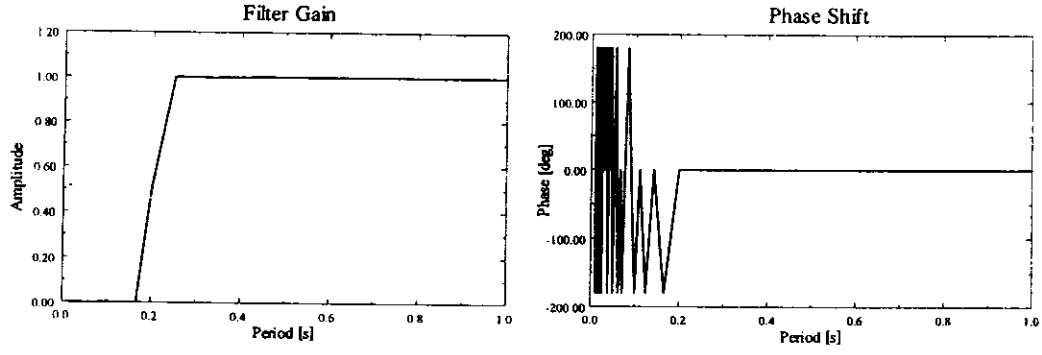

Fig. 23 Characteristics of digital filter employed in the post-processing

In Figure 23, the characteristics of the filter are described in detail. It is observed that the filter is very efficient in eliminating information below the 0.2 seconds threshold and that no phase shift is introduced in the response of the model. In Figure 24, the filtered and unfiltered responses of one of the test specimens are compared. From the observation of such plot, it becomes clear that appropriate filtering of the data is paramount in the process of extracting useful and meaningful information from this type of experiments.

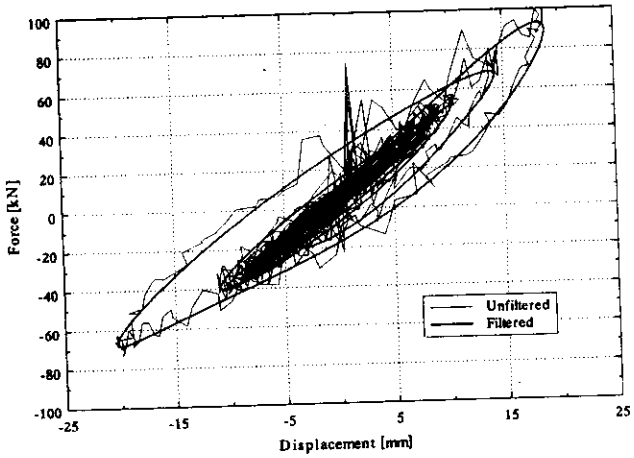

Fig. 24 Filtered and unfiltered response

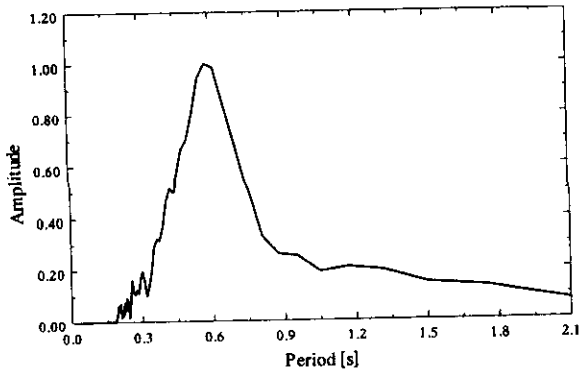

Fig. 25 Fourier spectrum of model SW3

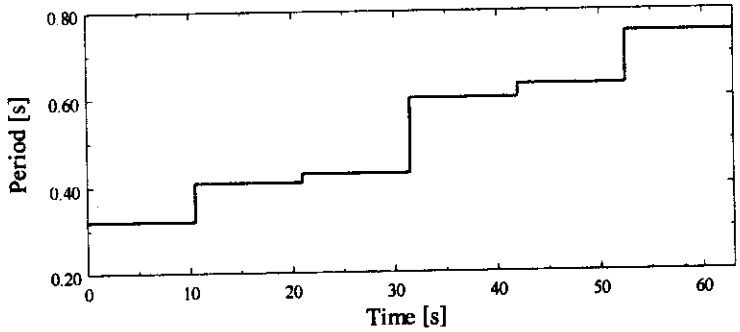

Fig. 26 Moving-window Fourier analysis of model SW4

2. Fourier Analysis

The Fourier spectrum of the response of the models was computed so that its inelastic period of vibration would become readily identifiable. Additionally, moving-window frequency analysis was also carried out to provide an insight into the period elongation (due to stiffness degradation) during the experiment. The plots corresponding to the tests of models SW3 and SW4 are given in Figures 25 and 26, respectively.

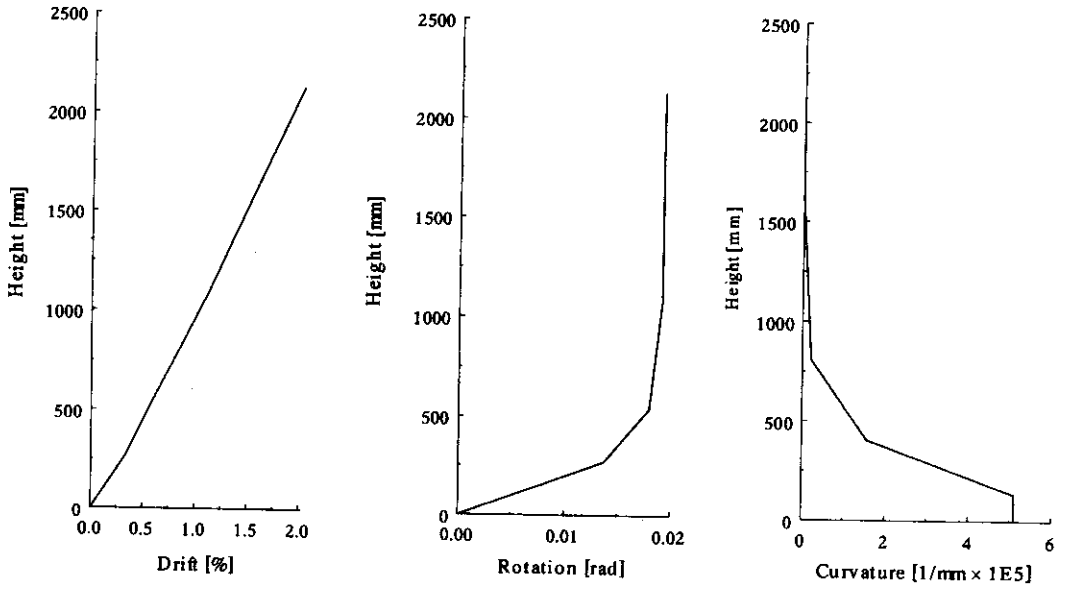

Fig. 27 Deformation profiles for model SW2 : (a) displacement (b) rotation (c) curvature

3. Deformation Profiles

The deformation profiles of the models in terms of displacement, rotation and curvature were plotted for any given time, as shown in Figure 27. Whilst horizontal displacement values were obtained directly from the output of the optical readers, both rotation and curvature values were computed through numerical manipulation of the vertical displacement readings. Note that rotation at any given point can be approximately obtained as the ratio between vertical displacement differential over section width, whilst curvature distribution is computed by considering that vertical displacements may be calculated through integration of curvature profile (a rectangular distribution between transducer locations was assumed).

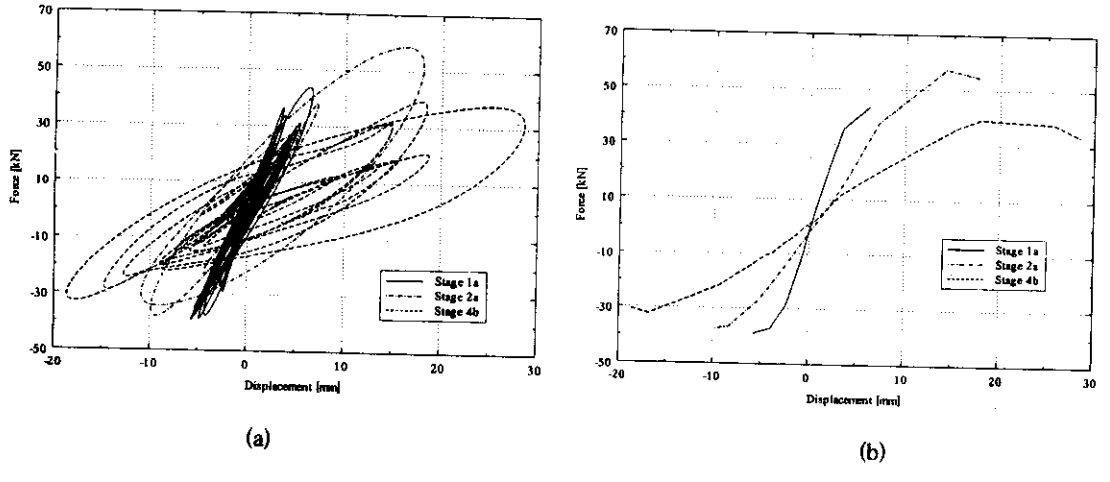

Fig. 28 Stage hysteretic curves and enveloped for model SW4

4. Hysteretic Curves and Envelopes

The hysteretic behaviour of each model was analysed in two different ways. Firstly, the response at each of the stages described above was plotted (Figure 28(a)) and analysed independently, followed by the computation of their envelopes (Figure 28(b)). This enabled a clear study of the variation in stiffness

and strength throughout the whole experiment. Thereafter, all stages were then adequately joined together and the total hysteretic curve and envelope were plotted and investigated (Figure 29). The latter was then used for comparison of response between different models and the evaluation of applied retrofitting schemes.

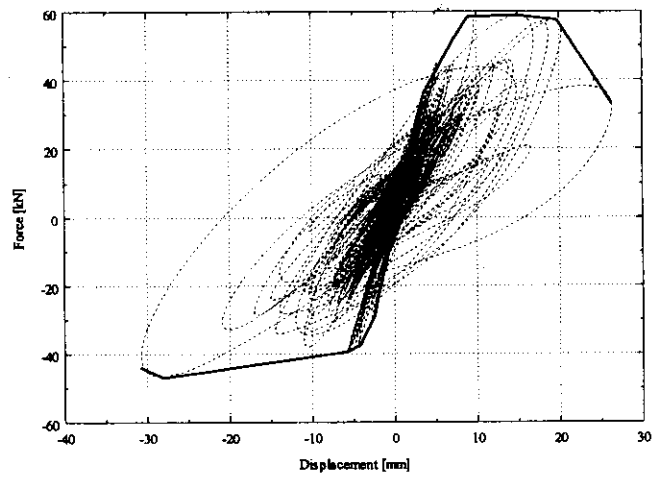

Fig. 29 Total hysteretic curve for model SW4

CLOSING REMARKS

Notwithstanding the significant developments, both at software and hardware levels, in the field of analytical simulation of the behaviour of structures under earthquake loading, physical testing is still an extremely valuable tool in this field. Indeed, final confirmation of new concepts and approaches to design, construction and structural intervention, require experimental verification under realistic loading conditions. On the other hand, analytical studies are central to the process of achieving results corroboration, due to the impracticality of investigating structural performance in a parametric fashion using labour-intensive and costly testing procedures, especially under dynamic loading. Therefore, development of advanced analytical modelling techniques and undertaking of highly controlled testing methods must go in tandem.

Amongst the three main types of testing methodologies available (static, pseudo-dynamic and dynamic), the use of shaking table testing is clearly the one providing the closest representation of the true dynamic effects that earthquakes impose on structures. However, such tests usually require the use of scaled models that may not be able to fully reproduce the behaviour of their prototype counterparts. Nonetheless, if large-scale specimens can indeed be used, shaking table test presents an ideal solution for final verification, under dynamic loading, of innovative structural solutions, which have already been previously studied and developed through the undertaking of simpler and cheaper static tests, complemented by extensive parametric numerical investigations.

Often, when testing large-scale reinforced concrete wall specimens, significant values of inertia masses are needed, either due to similitude requirements or to compensate for limitations in input capacity; thus, the use of external mass-support systems is necessary. A number of different schemes can be utilized, each of which present diverse advantages and drawbacks, thus providing a wide range of solutions to different types of research programmes with diverse objectives. In the case of cantilevered wall models, the use of either a system of stiff frames enclosing the test specimen or a fixed support structure outside the platform, can be deemed as an efficient solution for supporting mass blocks and transferring inertia loads to the specimens. The former presents advantages in controlling out-of-plane deformation, whilst the latter provides a very flexible solution in terms of assembly and disassembly of the test-rig and its application to different experimental studies. Further, for both cases, and in order to minimise friction effects, the use of roller bearings, as opposed to sliding pads, between the mass blocks and the support systems, is recommended.

Finally, full satisfaction of similitude laws may pose difficulties in terms of construction of small specimens and requirement of large masses. However, if the objectives of the tests do not include the exact reproduction of a real scenario, such scaling requirements may not be fully respected, thus rendering application of such testing methods much simpler and practical.

ACKNOWLEDGEMENTS

This research was funded by the European Commission through the Training and Mobility of Researchers (TMR) programme and by the Calouste Gulbenkian Foundation. The former provided support to the experimental work carried out at LNEC through the TMR Large-Scale Facilities Network - ECOEST II (European Consortium of Earthquake Shaking Tables). The analytical work, undertaken at Imperial College, was funded by another TMR network - ICONS (Innovative Concepts for Seismic Design of New and Existing Structures) - and by the Calouste Gulbenkian Foundation. Such financial support and the co-operation of the co-ordinators and members of the two networks is gratefully acknowledged. The author would also like to thank Prof. Elnashai, Dr. C.T. Vaz, Dr. A. Campos-Costa, Dr. R. Bairrão, Dr. E. Coelho, Dr. J. Duque and Ms. A. Martins for their technical assistance during the experimental programme at LNEC.

REFERENCES

1. Abrams, D.P. (1996). "Effects of Scale and Loading Rate with Tests of Concrete and Masonry Structures", Earthquake Spectra, Vol. 12, No. 1, pp. 13-27.
2. Ahsan, R., Maruyama, D. and Konagai, K. (2000) "Simulation of Non-Linear Soil-Structure Interaction in Shaking Table Tests", Proc. 3rd Japan-UK Workshop, Imperial College, London, U.K.
3. Aristizabal-Ochoa, J.D. and Clark, A.J. (1980). "Large-Scale Earthquake Simulation Tables", Proc. 7th World Conf. on Earthquake Engineering, Istanbul, Turkey, Vol. 7, pp. 157-164.
4. Bairrao, R. and Vaz, C.T. (2000). "Shaking Table Testing of Civil Engineering Structures – The LNEC 3D Simulator Experience", Proc. 12th World Conf. on Earthquake Engineering, Auckland, New Zealand, Paper No. 2129.
5. Bedell, R.J. and Abrams, D.P. (1983) "Scale Relationships of Concrete Columns", Research Report RS-83-02, Dept. of Civil, Environmental and Architectural Engineering, University of Colorado, Boulder, Colorado, U.S.A..
6. Bouwkamp, J.G., Penzien, J. and Rea, D. (1971). "Earthquake Engineering Facilities, University of California, Berkeley", Proc. 3rd European Symposium on Earthquake Engineering, Sofia, Bulgaria, pp. 693-700.
7. Carvalho, E.C. (1998). "Invited Lecture: Seismic Testing of Structures", Proc. 11th European Conf. on Earthquake Engineering, Paris, France, pp. 53-64.
8. CEN (1991). "European Prestandard ENV 1992-1-1: Eurocode 2 – Design of Concrete Structures, Part 1: General Rules and Rules for Buildings", Comite Europeen de Normalisation, Brussels, Belgium.
9. CEN (1996). "European Prestandard ENV 1998: Eurocode 8 – Design Provisions for Earthquake Resistance of Structures", Comite Europeen de Normalisation, Brussels, Belgium.
10. Crewe (1997). "Standardisation of Shaking Tables", Research Report ECOEST/PREC8-1, Laboratório Nacional de Engenharia Civil (LNEC), Lisbon, Portugal.
11. Duque, J. and Bairrao, R. (2000). "LNEC Experiences and Strategies in Earthquake Simulation. Recent Developments", Proc. 12th World Conf. on Earthquake Engineering, Auckland, New Zealand, Paper No. 2624.
12. Elnashai, A.S., Pilakoutas, K. and Ambraseys, N.N. (1988). "Shake-Table Testing of Small Scale Structural Walls", Proc. 9th World Conf. on Earthquake Engineering, Tokyo-Kyoto, Japan, Vol. 4, pp. 541-546.
13. Elnashai, A.S. (1992). "Effect of Member Characteristics on the Response of RC Structures", Proc. 10th World Conf. on Earthquake Engineering, Madrid, Spain, Vol. 6, pp. 3275-3280.
14. Elnashai, A.S. and Salama, A.I. (1992). "Selective Repair and Retrofitting Techniques for RC Structures in Seismic Regions", Research Report ESEE/92-2, Engineering Seismology and Earthquake Engineering Section, Imperial College, London, U.K.

15. Elnashai, A.S. and Pinho, R. (1998). "Repair and Retrofitting of RC Walls Using Selective Techniques", Journal of Earthquake Engineering, Vol. 2, No. 4, pp. 525-568.
16. Elnashai, A.S., Pinho, R. and Vaz, C.T. (2000). "Experimental Observations from Shaking-Table Tests on Selective Techniques for Repair and Strengthening of RC Walls", Proc. 12th World Conf. on Earthquake Engineering, Auckland, New Zealand, Paper No. 2245.
17. Farrar, C.R. and Baker, W.E. (1993). "Experimental Assessment of Low-Aspect-Ratio, Reinforced Concrete Shear Wall Stiffness", Earthquake Engineering and Structural Dynamics, Vol. 22, No. 5, pp. 373-387.
18. Inoue, N., Yang, K. and Shibata, A. (1997). "Dynamic Non-Linear Analysis of Reinforced Concrete Shear Wall by Finite Element Method with Explicit Analytical Procedure", Earthquake Engineering and Structural Dynamics, Vol. 26, No. 9, pp. 967-986.
19. Izzuddin, B.A. and Elnashai, A.S. (1989). "ADAPTIC: A Program for Adaptive Large Displacement Elastoplastic Dynamic Analysis of Steel, Concrete and Composite Frames", Research Report ESEE-89/7, Engineering Seismology and Earthquake Engineering Section, Imperial College, London, U.K.
20. Konagai, K. and Nogami, T. (1997). "Simulation of Soil-Structure Interaction on a Shaking Table", Geotechnical Special Technical Publication 64, American Society of Civil Engineers, pp. 91-106.
21. Lu, X.L. and Wu, X.H. (1996). "Shaking Table Test and Analysis of a New Type of Shear Wall with Seismic Control Device", Proc. 11th World Conf. on Earthquake Engineering, Paper No. 10.
22. Mathsoft (1998). "Mathcad 8 Professional - User Manual", MathSoft Inc.
23. Minowa, C., Hayashida, T., Abe, I., Kida, T. and Okada, T. (1996). "A Shaking Table Damage Test of Actual Size RC Frame", Proc. 11th World Conf. on Earthquake Engineering, Acapulco, Mexico, Disc 2, Paper No. 747.
24. Okada, T. (1978). "The Experimental Investigation of ERRCBC with Emphasis in the Use of Earthquake Response Simulators in Japan", Proc. of Workshop on Earthquake-Resistant Reinforced Concrete Building Construction, Univ. of California, Berkeley, California, U.S.A., Vol. III, pp. 1630-1651,.
25. Otani, S. and Sozen, M.A. (1972). "Behaviour of Multistory Reinforced Concrete Frames during Earthquakes", Research Report SRS-392, Structural Research Series, University of Illinois, Urbana, U.S.A.
26. Paulson, T.J. and Abrams, D.P. (1990). "Correlation between Static and Dynamic Response of Model Masonry Structures", Earthquake Spectra, Vol. 6, No. 3, pp. 573-591.
27. Pavese, A., Calvi, G.M., Vaz, C.T. and Bairrao, R. (1999). "Prove su Tavola Vibrante di Pile da Ponte", Proc. 9° Convegno Nazionale ANIDIS "L'Ingegneria Sismica in Italia", Torino, Italy (in Italian)
28. Pinho, R., Elnashai, A.S. and Vaz, C.T. (2000). "Shaking-Table Tests on Selectively Retrofitted RC Walls", Research Report ESEE-00/7, Engineering Seismology and Earthquake Engineering Section, Imperial College, London, U.K.
29. Rea, D. and Penzien, J. (1972). "Structural Research Using an Earthquake Simulator", Proc. Conf. of Structural Engineers Assoc. of California, Monterey, California, U.S.A.
30. Rogers, F.J. (1908). "Experiments with a Shaking Table", CSEIC Report, California State Earthquake Investigation Commission, Vol. 1, Part II, pp. 326-335.
31. Rothe, D. and König, G. (1988). "Behaviour and Modelling of Reinforced Concrete Structural Wall Elements", Proc. 9th World Conf. on Earthquake Engineering, Tokyo-Kyoto, Japan, Vol. VI, pp. 47-52.
32. Sozen, M.A., Otani, S., Gulkan, P. and Nielsen, N.N. (1969). "The University of Illinois Earthquake Simulator", Proc. 4th World Conf. on Earthquake Engineering, Santiago, Chile, Vol. III, pp. 139-149.
33. Yabana, S., Kanazaca, K., Ohmiya, Y., Taniguchi, H. and Kambayashi, A. (1996). "Shaking Table Tests of Earthquake Resisting Walls", Proc. 11th World Conf. on Earthquake Engineering, Paper No. 456.
34. Yamada, S., Matsumoto, Y. and Akiyama, H. (2000). "Full-Scale Shaking Table Test of Structural Elements Using the Inertial Loading Equipment", Proc. 3rd Japan-UK Workshop, Imperial College, London, U.K.